Accepted Manuscript

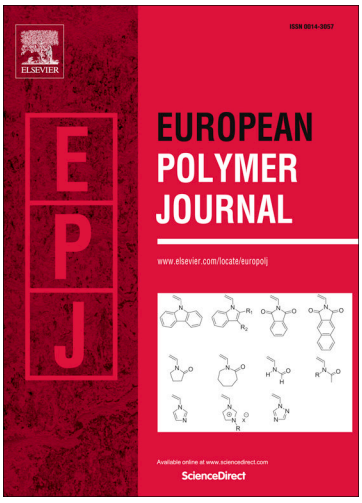

Main structural features of graphene materials controlling the transport properties of epoxy resin-based composites

R. Sánchez-Hidalgo, V. Yuste-Sanchez, R. Verdejo, C. Blanco, M.A. Lopez-Manchado, R. Menéndez

PII: S0014-3057(17)32287-5
DOI: https://doi.org/10.1016/j.eurpolymj.2018.02.018
Reference: EPJ 8292

To appear in: *European Polymer Journal*

Received Date: 21 December 2017
Revised Date: 5 February 2018
Accepted Date: 11 February 2018

Please cite this article as: Sánchez-Hidalgo, R., Yuste-Sanchez, V., Verdejo, R., Blanco, C., Lopez-Manchado, M.A., Menéndez, R., Main structural features of graphene materials controlling the transport properties of epoxy resin-based composites, *European Polymer Journal* (2018), doi: https://doi.org/10.1016/j.eurpolymj.2018.02.018

Main structural features of graphene materials controlling the transport properties of epoxy resin-based composites

R. Sánchez-Hidalgo[1,2], V. Yuste-Sanchez[2], R. Verdejo[2], C. Blanco[1], M.A. Lopez-Manchado[2*], R. Menéndez[1]

[1]*Instituto Nacional del Carbón, INCAR-CSIC, Apartado 73, 33080 Oviedo, Spain*

[2]*Instituto de Ciencia y Tecnología de Polímeros, ICTP-CSIC, C/ Juan de la Cierva 3, 28006-Madrid, Spain*

Abstract

Graphene materials (GMs) are deeply studied as nanoreinforcements of polymer matrices, especially for epoxy matrices. Here, we analyze the effect of GMs on the transport properties of a poly(bisphenol A-co-epichlorohydrin) resin. In particular, we focus on the effect of the morphology, chemical composition and structure of different GMs obtained by varying the reduction temperature of the thermal/exfoliation treatment of graphite oxide synthesized by a modified Hummers method. The dispersion degree of the GMs was studied by microscopy techniques, showing a strong dependence on the specific surface area and chemical composition of the graphene material. The transport properties imposed different requirements on GMs. The thermal conductivity benefited from a high aromatic restoration. Meanwhile, the electrical conductivity required the right balance of filler/matrix interaction and aromatic restoration.

Keywords: Graphene; Epoxy; Transport properties; Polymer nanocomposites

*Corresponding author: lmanchado@ictp.csic.es
Tel: +34 912587424

1. Introduction

The intrinsic properties of epoxy resins, such as strong adhesion, mechanical behavior and chemical resistance, make them suitable for a wide spectrum of applications in diverse areas such as adhesives, paints and coatings, aerospace and electrical systems [1]. Nonetheless, different carbonaceous materials, such as carbon nanotubes [2], and fullerenes [3], have been incorporated in order to improve the mechanical or transport properties of epoxy resins. Graphene is a 2D material with a one-atom thick planar sheet of sp^2 bonded carbon atoms in a hexagonal lattice with excellent properties like Young's modulus (1 TPa) [4], high electrical (6000 S cm^{-1}) and thermal conductivity (5000 W m^{-1} K^{-1}) [5] and a good fracture toughness performance [6]. Therefore, it is not only expected to improve the mechanical performance of epoxy resins but also to bring new properties like enhanced electrical and thermal conductivities [7, 8].

In recent years, several studies have been reported regarding the properties of epoxy resin based composites filled with different graphene materials (GMs), e.g. graphene oxide [9, 10], reduced graphene oxide [11], graphene nanoplatelets [12, 13] or thermally reduced graphene oxide [8, 14]. Although a detailed review can be found about the effect of sheet size focusing on their mechanical properties [15], to our knowledge, there are no detailed studies concerning the effect of the structure or morphology of the different GMs on the transport properties of the resin composite.

Our research group has developed a production method that enables the control of different GM characteristics, such as specific surface area, oxygen content and lateral size, by tuning the exfoliation/reduction temperatures of the graphite oxide and the parent graphite used [16-18]. In the present study, four graphene materials were selected

to evaluate the role of their structure, morphology and chemical composition on the transport properties of epoxy-graphene resin composites.

Thus, the objectives of this study are: (i) a deep characterization of the graphene materials obtained by the methodology developed by our research group (ii) to study the dispersion behavior of the different graphene materials (GMs) in the epoxy resin; (iii) to evaluate the transport properties of the composites reinforced with the different GMs as a function of their chemical and structural composition and the degree of dispersion of graphene.

2. **Experimental**

2.1. Preparation of graphite oxide (GrO) and thermally reduced graphene oxides (TRGOs)

GrO was prepared from synthetic graphite (Sigma Aldrich < 20 μm Ref. 282863) using a modified Hummers' method [19]. Briefly, concentrated H_2SO_4 (360 mL) was added to a mixture of graphite (7.5 g) and $NaNO_3$ (7.5 g). Subsequently, $KMnO_4$ (45 g) was slowly added in small quantities to keep the reaction temperature below 20 °C. The solution was heated to 35 °C and stirred for 3 h. Finally, 3% H_2O_2 (1.5 L) was slowly added to the reactor. The reaction mixture was stirred for 30 min and, subsequently, centrifuged (4000 rpm for 10 min) and the supernatant was decanted away. Then, the remaining solid material was washed with 500 mL of deionized water and centrifuged again. This process was repeated until neutral pH. The bulk resulting product was vacuum dried and then ground to obtain graphite oxide powder (GrO) [19].

Thermally reduced graphene oxides (TRGOs) were obtained at different temperatures. Initially, graphite oxide (GrO) was subjected to a flash pyrolysis exfoliation at 300 ºC (TRGO-300) in a vertical tube furnace under a N_2 atmosphere (100

mL min^{-1}) [16]. The obtained TRGO-300 was immediately collected after the exfoliation process and natural cooled to room temperature under N_2 atmosphere. The resultant exfoliated sample was submitted to a thermal treatment at 1000 °C (TRGO-1000) in a horizontal tubular furnace under a N_2 atmosphere (100 mL min^{-1}) and with a heating rate of 5 °C min^{-1} up to the selected final temperature. This temperature was maintained for 1h. The treatment at 2000 °C was performed in a graphitization furnace (Pyrox VI 150/125) under an Ar atmosphere (3 L min^{-1}) at a heating rate of 5 °C min^{-1} up to 800 °C and, then, at 10 °C min^{-1} up to 2000 °C. This temperature was maintained for 1 h [19]. Both, TRGO-1000 and TRGO-2000 were natural cooled to room temperature inside the furnace under their respective inert atmospheres. The obtained samples were labeled as TRGO-300, TRGO-1000 and TRGO-2000, respectively.

2.2. Preparation of resin-based composites

Poly(Bisphenol A-co-epichlorohydrin) resin (405493) and diethylenetriamine curing agent (D93856) were purchased from Sigma-Aldrich. The TRGOs were dispersed in the epoxy resin using a three-roll calender (EXAKT 80E). Different TRGO contents were studied: 0.25, 0.5, 1, 2, 3 and 4 wt.%, which corresponds to 0.13, 0.26, 0.52, 1.04, 1.56 and 2.06 vol. % respectively, calculated using a density value of GM of 1.92 g/cm^3. In order to obtain a good dispersion of the TRGOs in the epoxy matrix, a method based in three cycles was used. The parameters of this method (roller gap, velocity and time) are summarized in Table 1. The liquid formulations containing GMs and epoxy resin were mixed immediately after the calender mixing process with the curing agent in a mixing ratio (epoxy: hardener) of 100:12.

Table 1. Calender dispersion protocol

	Gap 1 (μm)	Gap 2 (μm)	Velocity (rpm)	Time (min)
Cycle 1	100	50	150	10
Cycle 2	50	25	200	10
Cycle 3	25	5	250	30

The mixture was degassed for 10 min at room temperature in a vacuum chamber and then poured into silicone molds for its thermal and electrical characterization. The samples were cured in an oven at 70 ºC for 60 min and then, post-cured at 140 ºC for 90 min.

2.3. Characterization

X-ray diffractograms of the graphene materials were recorded in a Bruker D8 Advance diffractometer. The radiation frequency used was the $K_{\alpha 1}$ line from Cu (1.5406 Å), with a power supply 40 kV and 40 mA. All the XRD patterns were obtained at steps of 0.01 and intervals of 6 s per step. The crystallite size along the c-axis (L_c), and the crystallite size along a-axis (L_a) were obtained by fitting respectively the (002) and (100) reflections of XRD patterns using the Scherrer equation [20]. A pseudo-Voigt function was used in order to obtain the best fit of (100) reflection of the XRD patterns. The number of graphene layers was estimated from (L_c/d_{002}) +1 [21].

The oxygen content of the samples was determined in a LECO-TF-900 furnace coupled to a LECO-CHNS-932 microanalyzer. The analysis was performed using 1 mg of ground sample. The results were calculated from an average of the values of three batches with an experimental error < 3% of the absolute value.

XPS analysis of graphene materials were carried out on a SPECS system operating under 107 Pa connected to a MgKa X-ray source (100 W). All the spectra were energy calibrated by assigning 284.5 eV to the C1s binding energy of the 'graphitic' peak. In

order to evaluate the functional groups present in the samples, the XPS C1s peaks were curve-fitted using pseudo-Voigt functions having 80% Gaussian and 20% Lorentzian character [22]. The binding energy profiles were deconvoluted as follows: undamaged structures of Csp^2 - hybridized carbon (284.5 eV), damaged structures or Csp^3 - hybridized carbons (285 eV), C–OH groups (285.7 eV), C-O-C functional groups (287 eV), >C=O groups (287.5 eV), C(O)OH groups (288.7 eV) and π-π^* transition (290 eV) [23, 24].

Raman spectra were recorded from 750 to 3500 cm^{-1} on a Renishaw 2000 Confocal Raman Microprobe (Rhenishaw Instruments, England) using a 514.5 nm argon ion laser. To ensure the consistency of the results, at least five measurements were carried out for each sample. All spectra were corrected using the Si band at 520 cm^{-1}. The resulting Raman spectra were evaluated with a fitting method using two Gaussian functions and three pseudo-Voigt profiles in the first-order region from 800 cm^{-1} to 2000 cm^{-1}. The Raman spectra were normalized and then the baseline of the spectrum was subtracted using Shirley correction before fitting.

The specific surface area was calculated from the N_2 adsorption isotherms at 77 K using the BET equation. The analysis was carried out in ASAP 2020 Micromeritics equipment using over 100 mg of sample for each test. Samples were degassed at 300 ºC for 3 h under vacuum prior to the test. The error of the experiment data found was less of 8% in all cases.

The dispersion of the different graphene materials into the epoxy matrix (uncured) was studied by optical microscopy with a NIKON DS–Fi2 microscope. On the other hand both, the structure of graphene materials and their dispersion in the cured samples, were studied using TEM JEOL 2000 EX-II instrument operating at 160 keV.

The thermal conductivity of uncured resin dispersions was studied with KD2-Pro thermal analyzer at 25 ºC. The error of the experiment data was found to be less than 1% in all cases. The thermal diffusivity (α) of cured samples was measured on a laser flash thermal analyzer (NETZSCH-LFA 447 Microflash, Germany). The analyzed samples were square-shaped with dimensions 10x10x2 mm.

Electrical conductivity of the cured composites was determined on an ALPHA high-resolution dielectric analyzer (Novocontrol Technologies GmbH) with voltage amplitudes of 1 V ac and 0 V dc over a frequency range of 10^{-1} – 10^{7} Hz at room temperature. Five cylindrical samples, 20 mm diameter and ~1.5 mm thickness, were measured between two parallel gold-plated electrodes.

3. Results and discussion

3.1. Characterization of the graphene materials

The main features of the different graphene materials were investigated prior to the preparation of the composites. The flash pyrolysis exfoliation of GrO at 300 °C causes a reduction of the oxygen content from 49.3 to 30.8 wt.% obtaining a partially reduced graphene oxide (TRGO-300). Beyond 1000 ºC, the oxygen content decreases drastically (1 wt.%) and it practically disappears in the case of the graphene obtained at 2000 ºC (0.2 wt.%) (Table 2). The type of oxygen functionalities present in the graphene materials was studied by XPS. Fig. S1 presents the C_{1s} core level spectra of the different samples, which is in all cases an asymmetric band that can be fitted by seven components. Table 2 shows the percentage of the different species.

Table 2. Oxygen content determined by elemental analysis and fitted results of C1s core level XPS spectra

Sample	O[a] (wt.%)	Csp^2 (%)	Csp^3 (%)	C-OH (%)	C-O-C (%)	>C=O (%)	COOH (%)	π- π*
GrO	49.3	6.0±1.3	35.8±5.0	6.1±1.2	27.7±2.3	11.5±5.9	13.0±3.6	0.0
TRGO-300	30.8	43.3±2.2	24.5±1.0	10.3±1.7	11.6±0.7	3.9±0.8	6.4±0.2	0.0
TRGO-1000	1.0	67.8±0.3	15.1±0.3	11.7±1.2	0.0	4.2±0.2	0.0	1.2±0.1
TRGO-2000	0.2	82.7±1.3	10.1±0.3	5.9±1.3	0.0	0.0	0.0	1.3±0.2

[a] *Determined by elemental analysis*

The C1s core-level spectrum of GrO shows a bimodal distribution. Most of the carbon atoms present sp^3 hybridization due to the covalent bonds with oxygen atoms formed during the highly oxidative Hummers reaction. Most of the oxygen groups in this sample have been assigned to epoxy, carbonyl and carboxylic groups in agreement with results previously reported [24-26]. TRGO-300 shows an increase in the carbon sp^2 content as a result of the removal of the most labile oxygenated groups such as carboxylic, epoxy and carbonyl groups [27-29]. At higher annealing temperatures (1000 °C), the epoxy and carboxylic groups were entirely removed, being the remaining oxygen mainly in the form of hydroxyl groups [19, 23]. As a consequence of the aromatic restoration, a weak band appears around 290.5 eV which is assigned to π-π^* transition. Meanwhile, the asymmetric band of the core-level C1s of the TRGO-2000 can be fitted to only four bands: a very intense one corresponding to aromatic carbon (sp^2) and the other three less intense, corresponding to the carbon with sp^3 hybridization, hydroxyl groups and π-π^* transition, respectively [19, 23].

The XRD patterns also show significant differences between the samples. GrO shows an XRD pattern with the characteristic strong and sharp signal at $2\theta = 10^o$ [19]. Thermal exfoliation/reduction of GrO produces aggregated and randomly packed layers with a broad and low intensity diffracted signal centered at 23º-26º (Fig. S2). The

broadening of the peak in TRGO-300, could be due to the abrupt process of flash pyrolysis exfoliation favoring the removal of water molecules and more labile oxygen groups such as carboxylic groups. Compared to other diffractograms reported in the literature for this reduction temperature [29], no significant peaks were found at 10º-15º due to an effective exfoliation/reduction process. As a consequence of this thermal exfoliation/reduction, the interlaminar distance d_{002} decreases from 0.852 nm, in the case of GrO, to 0.371 nm. The L_c value found for TRGO-300 is significant lower compared to GrO, which indicates the decrease in the periodicity in the c-axis as a result of the thermal exfoliation treatment. Furthermore, there is a drastic decrease of the number of layers, estimated from L_c, after the exfoliation process, resulting in ~4 layers for TRGO-300.

When increasing the temperature of the thermal treatment up to 1000 ºC, an interlaminar distance of 0.360 nm was calculated from the peak centered at 24º. In this case the broad peak was ascribed to the presence of hybrid structures with sp^2 and sp^3 hybridization [29].

The peak in TRGO-2000 is more intense and sharper due to a significant increase of the crystalline quality as a result of the higher temperature of the treatment. The reflection (002), centered at 26º, corresponds to the interlaminar distance of 0.341 nm, close to that of pristine graphite [30]. The sharp peak reveals the presence of large graphitic domains with a large crystallite size in the c-axis (6.10 nm) and crystallite size in the a-axis (11.56 nm) (Table 3). Hence, a significant restoration of aromatic domains was achieved with this high annealing treatment corroborating the XPS results.

Table 3. BET surface area and XRD data of the graphene materials

Samples	S_{BET} (m^2/g)	XRD			
		d_{002} (nm)[a]	L_c (nm)[b]	n[c]	L_a (nm)[d]
GrO	45	0.852	9.60	12	26.20
TRGO-300	251	0.371	1.18	4	7.31
TRGO-1000	467	0.360	1.39	5	8.43
TRGO-2000	161	0.341	6.10	19	11.56

a interlaminar distance; b crystallite size in the c-axis; c number of layers estimated by XRD from (L_c/d_{002})+1; d crystallite size in the a-axis calculated from (100) reflection.

As the aromatic network is restored, morphological changes occur in the structure causing low sheet roughness, as observed by TEM (Fig. 1). Thus, the morphological changes achieved in the graphene sheets causes the stacking of the layers, increasing the estimated number of layers to 19. Therefore, the used protocol, i.e. flash pyrolysis exfoliation and subsequent thermal reduction, produces more exfoliated graphene materials with fewer number of layers compared to other GMs obtained in previous studies [19].

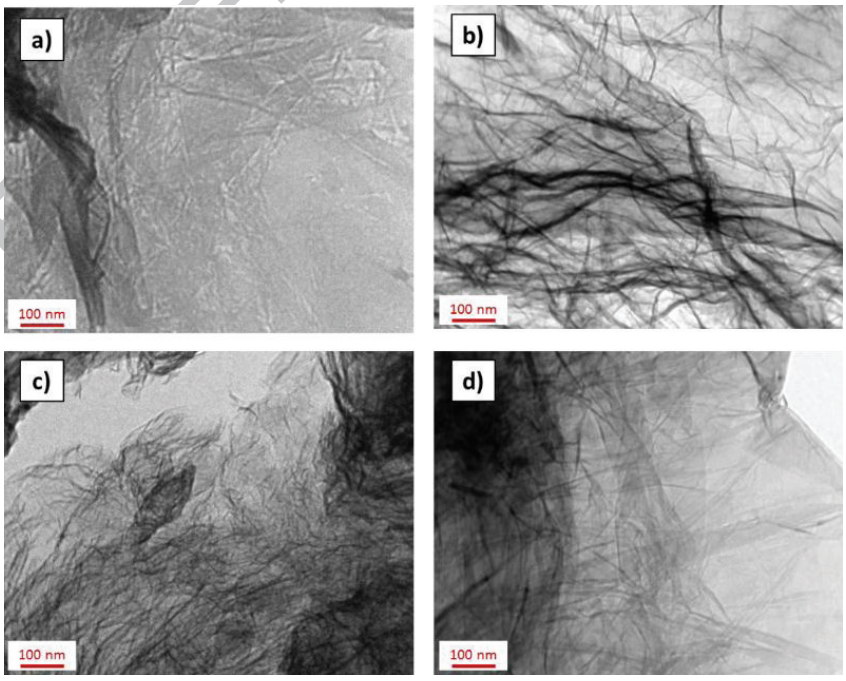

Figure 1. TEM images of a) GrO b) TRGO-300 c) TRGO-1000 and d) TRGO-2000

Raman spectroscopy reflects the significant structural changes occurred during the annealing treatment. The first order Raman spectra of graphene materials shows a characteristic G band, around 1580 cm^{-1}, which is due to the vibration of the aromatic domains in the basal plane assigned to the zone center phonons of E_g symmetry. The peak at 1360 cm^{-1} (D-peak) is attributed to phonon A_{1g} symmetry [31]; while the peak around 1615 cm^{-1} (D'-peak) is ascribed to the disorder produced by crystal defects, such as atomic vacancies (Fig. 2) [32]. Moreover, two additional peaks were introduced to the fitting of these first-order Raman spectra; the I-peak, at around 1200 cm^{-1}, related to disordered graphitic lattice by sp^2-sp^3 bonds at the edges of network [33], and the D''-peak, at 1500 cm^{-1}, related to the amorphous lattices in carbon materials [34].

Table 4. Intensity ratios of characteristics peaks after deconvolution of Raman spectra

Samples	I_D/I_G	I_I/I_G	$I_{D''}/I_G$	$I_{D'}/I_G$
GrO	1.12±0.03	0.13±0.01	0.37±0.03	0.26±0.03
TRGO-300	1.21±0.04	0.11±0.02	0.38±0.09	0.34±0.03
TRGO-1000	1.48±0.05	0.13±0.02	0.23±0.06	0.25±0.01
TRGO-2000	0.18±0.08	0.00±0.00	0.04±0.01	0.10±0.03

The intensity ratio of D and G bands provides information on the crystallinity of the materials and the disorder in the basal-plane [35]. GrO spectrum exhibits a broad and prominent D band, mainly due to the presence of large amounts of oxygenated functional groups and atomic vacancies (I_D/I_G=1.12). The I_D/I_G ratio increases with the annealing temperature to reach a maximum with TRGO-1000 (I_D/I_G=1.48). Even though at this temperature, most of the oxygenated groups (mainly epoxy ones) have been removed the high value measured could be explained considering the small average size of the restored aromatic domains in the basal plane [19]. Moreover, a significant

decrease of D"-peak was observed (Table 4), corroborating the partial aromatic restoration in the basal plane. Beyond this temperature, as in the case of TRGO-2000, the aromatic domain is significantly restored and, hence, the I_D/I_G ratio decreases to 0.18, which is close to pristine graphite values [35]. Additionally, the almost disappearance of the I and the significant decrease of D" and D' peaks is in agreement with the reduction of edge defects and atomic vacancies as a consequence of the high temperature of the thermal treatment.

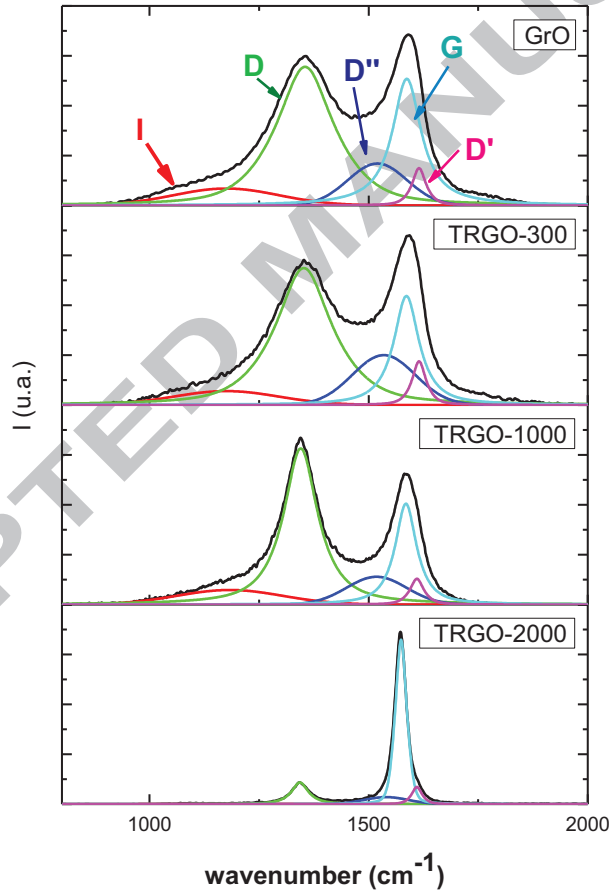

Figure 2. Raman spectra of GrO and TRGOs

The morphological and structural changes of the graphene materials previous discussed (Fig. 1) were also revealed by the BET results (Table 3). These values vary from 45 m^2/g for GrO to a maximum of 467 m^2/g for TRGO-1000, due to the abrupt expansion of the graphite oxide layers caused by the removal of occluded water and the more labile oxygen groups.

As discussed above, the reduction treatment at higher temperatures results in tightly packed material (TRGO-2000) due to the large aromatic domain restauration (Table 2). This fact favours the re-stacking of the material by π-π* interactions, thus explains the increase of L_c value and a decrease in the BET specific surface area (Table 3). Due to these morphological changes, a lower roughness of the layers compared to the other TRGOs was observed by TEM (Fig. 1d).

These four graphene materials with notable morphological, chemical and structural differences were further used as reinforcement in epoxy resin to evaluate not only their dispersion in the polymer matrix but also their transport features.

3.2. The effect of GMs morphology on their dispersability into the epoxy resin matrix

Prior to the study of the transport properties of graphene filled epoxy composites, the dispersion of GrO and the TRGOs into the uncured epoxy resin was investigated by optical microscopy. The micrographs show a homogeneous dispersion of the graphene materials in the resin (Fig. 3), with significant differences among them.

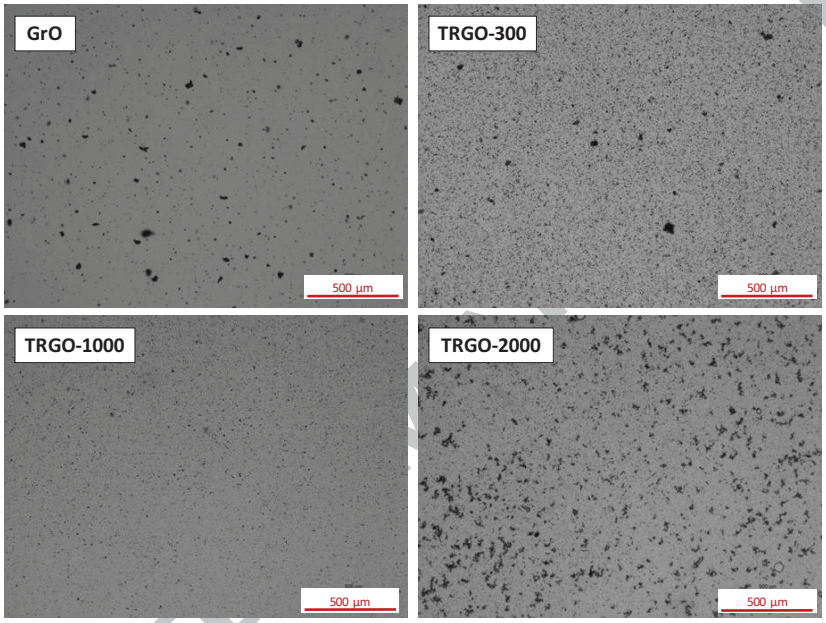

Figure 3. Neat resin dispersion with 0.13 vol. % of GMs

While the different behavior in the dispersion could be explained based on the BET specific surface areas and the oxygen content, it appears that the dominant factor is the BET surface area. It would be expected that both GrO and TRGO-300, with a high oxygen content, *i.e.* more polar, would readily dispersed in the epoxy resin, also polar. However, both materials show the presence of agglomerates, being smaller in the case of TRGO-300 due to the larger BET surface area compared to GrO. The formation of large agglomerates of graphene oxides has previously been observed [36] and has also been ascribed to the weak interactions between matrix and particle. Comparing the

dispersion behavior of the different TRGOs, the most homogeneous dispersion in the resin corresponds to TRGO-1000, followed by TRGO-300 and, then TRGO-2000, which is directly related to their BET surface area (467, 251, and 161 m^2/g, respectively). This dispersion trend with respect to the specific surface area is maintained with the concentration of the GMs, but we observed an increase of the size of the aggregates (Figure S4).

Therefore, BET surface area is the key factor on the dispersion degree of TRGOs since it can allow the intercalation of the epoxy resin chain between the layers, preventing the formation of agglomerates.

The dispersion after curing was studied by TEM (Fig. 4). The curing protocol does not seem to alter the dispersion degree observed by optical microscopy. Again, the best dispersion is achieved for TRGO-1000 and the most prominent aggregates are observed in GrO and TRGO-2000.

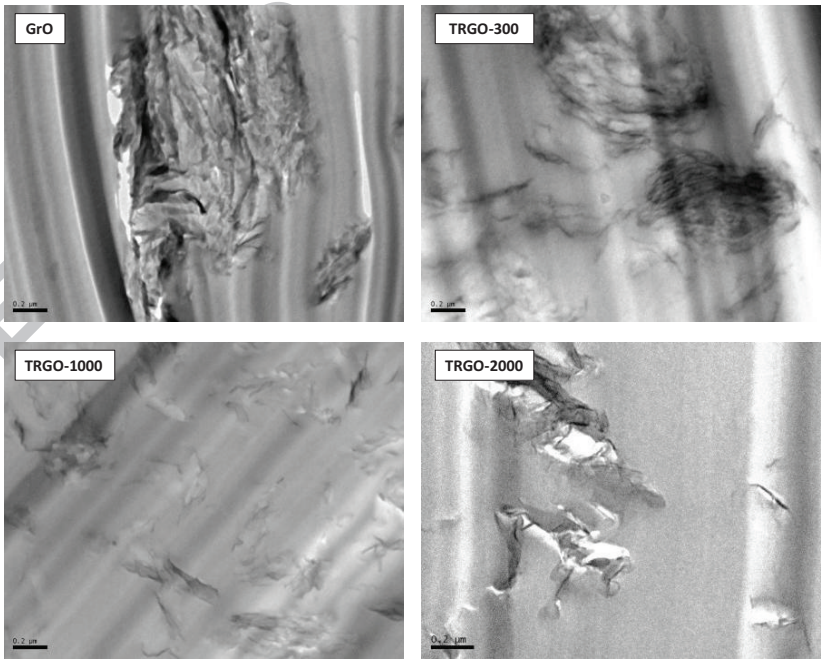

Figure 4. Representative TEM images of the 2.06 vol. % GMs/epoxy composites showing the effect of chemical composition and BET surface area on the dispersion

3.3. Electrical conductivity of the composites

Impedance spectroscopy, as a function of frequency, of the obtained composites was also studied and the conductivity calculated from the modulus of the complex impedance and the sample geometry. The dielectric properties of the GMs/epoxy composites at different loading nanofiller contents are represented in Figure 5. The conductivity spectra present the typical behaviour of two-phase systems: below a concentration, the AC conductivity is linearly dependant with the frequency, and, above it, the conductivity presents a plateau up to a critical frequency, where the dispersion regime is again observed. This behaviour is commonly described by the percolation theory [37], which states the existence of a concentration, or percolation threshold, where the filler forms a conductive network. The critical frequency is ascribed to the dominant character of the capacitor admittance of the insulating matrix. In a composite, the AC conductivity is composed of two terms:

$$\sigma_{AC}^{*} = \sigma_{DC} + A\omega^{s} \quad \text{(I)}$$

where σ_{DC} is the direct current conductivity, A is a pre-exponential factor and s is an experimental parameter with values between 0 and 1 [38]. For insulating materials s = 1. Hence, from Eq. I, the DC conductivity values can be obtained by extrapolating the broadband AC conductivity to 10^{-1} Hz.

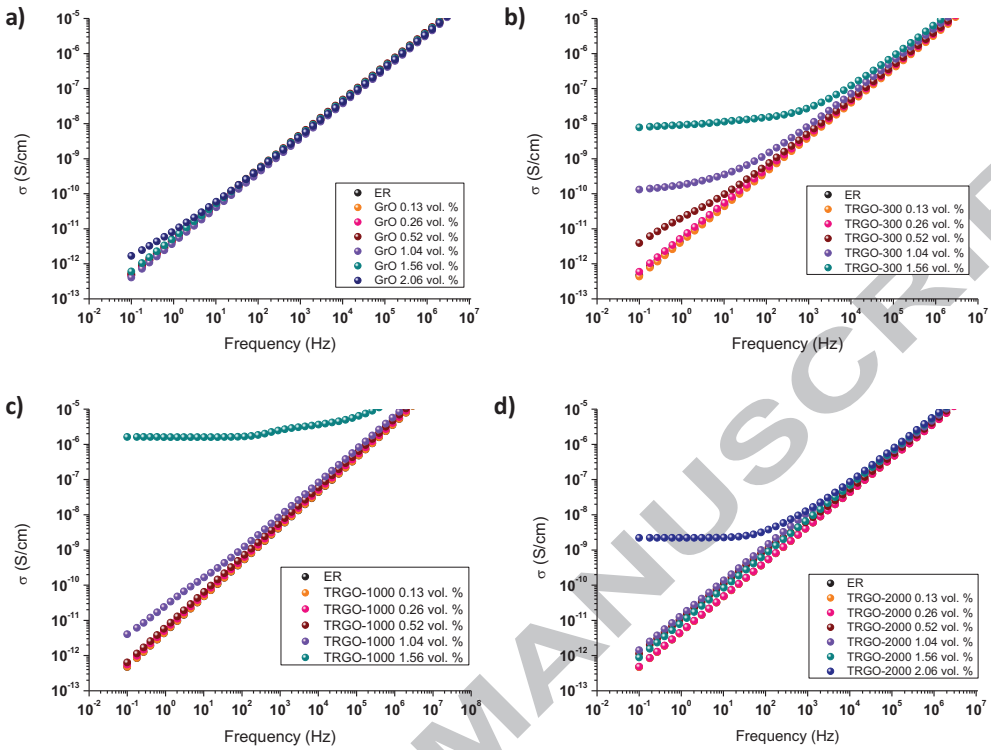

Figure 5. AC electrical conductivity versus frequency of a) GrO b) TRGO-300 c) TRGO-1000 and d) TRGO-2000 composites.

Figure 6 shows DC conductivity for the composites studied as a function of nanofiller content. The dotted areas show the electrical percolation region for each type of GM. The electrical percolation is attained at lower loading fractions, 0.8 vol.% for TRGO-300 while TRGO-1000 at 1.6 vol.% forms the most effective filler network, resulting in high values of electrical conductivity. The lower percolation threshold of TRGO-300 compared to TRGO-1000 could be related to a good interaction between the TRGO-300 and the matrix that would eliminate micro-voids that hinder the formation of a conductive network [39, 40]. Meanwhile, the high electrical conductivity of TRGO-1000 can be ascribed to a balanced combination of two critical parameters: a sufficient aromatic restoration of the basal plane (Table 2) and the large BET surface area (Table

3), which results in a good dispersion state. Such dispersion is considered to enable the electrical conduction via tunnelling between adjacent graphene material layers [41]. The GrO composites do not show significant changes in electrical conductivity, which indicates that the percolation threshold is not reached. The oxygen groups in the basal plane, the large aggregates and low BET surface area of GrO would hinder the electrical conductivity of the fillers and their interconnection.

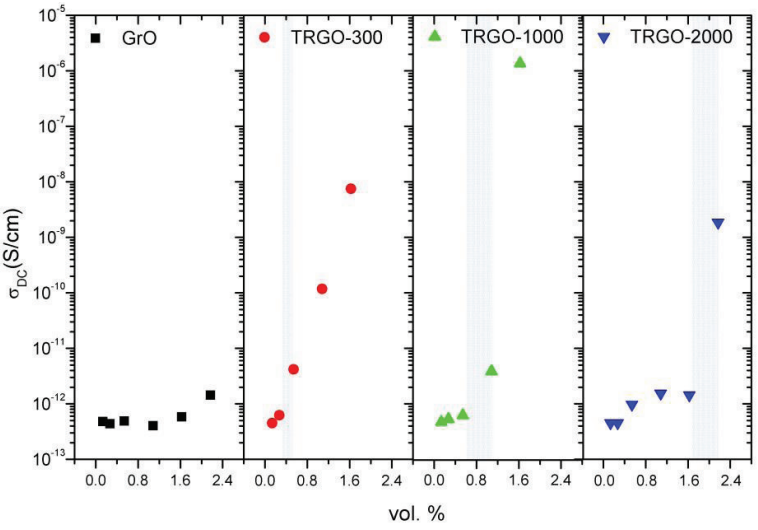

Figure 6. DC electrical conductivity of the GMs/epoxy composites as a function of the filler content

It could have been expected that TRGO-2000, with the most aromatic restored lattice, would be the ideal GMs-filler, as observed in our own previous work [42]. This study showed that the electrical conductivity depended on the reduction temperature of the GMs, reaching its maximum with graphene material reduced at 2000 °C. This conflicting result could be due to the different epoxy matrices used for the studies and, hence, differences on the filler/matrix interaction and/or the different initial graphite source use for the oxidation. Therefore, to study the first option, we analyzed the

possible interaction of the hardener and oxygen groups of the GMs. Hence, we reacted the graphene materials with diethylenetriamine (DETA) in the same conditions as for the curing process. XPS measurements of the reacted materials revealed the formation of covalent bonds C-N in all cases except for TRGO-2000 (Table 5).

Table 5. Atomic percentage of C, O and N of the functionalized GMs

Sample	C (%)	O (%)	N (%)
FGrO	76.0	19.3	4.7
FTRGO-300	82.4	14.4	3.2
FTRGO-1000	94.9	4.5	0.6
FTRGO-2000	96.8	3.2	--

The possible reactions are epoxide ring opening and reduction of carbonyl groups [43, 44] (Fig. 7). The large quantity of oxygen in GrO and TRGO-300 (in the form of epoxy and carbonyl groups in the basal planes) is susceptible to be attacked by the amine groups of hardener agent. Although functionalization of the carbon nanofillers can reduce their intrinsic conductivity, it also results in a good dispersion state and, as already discussed, more electrical percolation pathways [39, 40]. The oxygen groups of TRGO-1000 are mostly hydroxyl groups in the basal plane [23]. However, there are still enough remaining carbonyl groups susceptible to be attacked by the amine. Meanwhile, TRGO-2000 showed no formation of C-N bonds, due to the lack of oxygen groups amenable to amination. We are currently analyzing the possible interactions with the epoxy resin used on our previous work and the effect of the starting graphitic material to corroborate these assumptions.

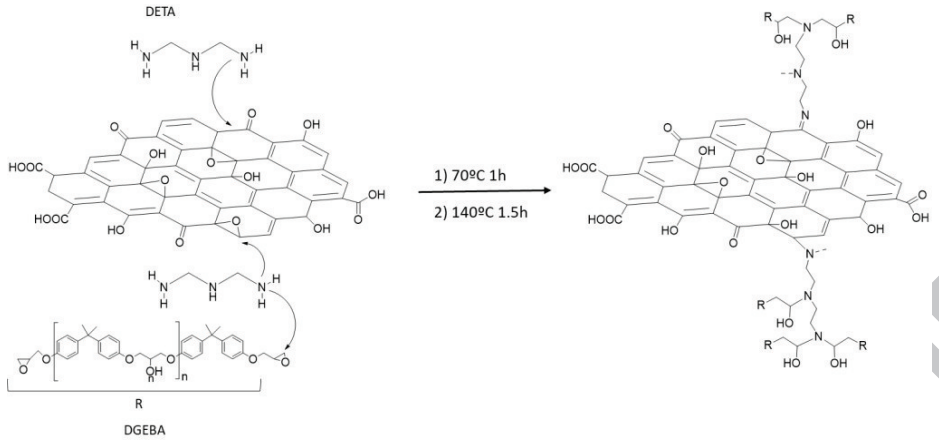

Figure 7. Schematic representation of possible reaction of oxygen groups of GMs and DETA

Hence, the BET surface area and oxygen functionalization of GMs play a decisive role in the formation of the percolation network and, subsequently, in the electrical properties achieved on epoxy composites.

3.4. Thermal conductivity of the uncured nanofluids and diffusivity of the cured composites

The thermal conductivity of composites containing carbon fillers is known to depend on the interfaces between the fillers and matrix, the dispersion of the fillers, and the intrinsic thermal conductivity of the fillers [45]. Likewise, the thermal conductivity of films of graphene oxide reduced at different temperatures has also been reported to vary with the annealing temperature. Renteria et al. and Huang et al. showed an upward trend of the thermal conductivity with the reduction temperature, reporting in-plane conductivity values from about 14 to 61 W m^{-1} K^{-1} at room temperature for 300 °C and 1000 °C annealing temperatures, respectively [46], and 106 W m^{-1} K^{-1} and 826.0 W m^{-1} K^{-1} for 1200 °C and 2800 °C annealing temperatures, respectively [47]. The combination of these factors makes the development of high thermal conductivity

polymer composites a challenging endeavor and limited studies can be found in the literature on the subject. Several studies on the thermal conductivity of GMs/epoxy composites have showed its dependency with the GM characteristics, such as size [48], waviness [49] and number of layers [50] and surface functionalization [51-53]. Here, we analyze the combined effect of several of those factors through the annealing temperature of thermally reduced graphene on uncured and cured samples.

Initially, the thermal conductivity of the uncured state was determined at room temperature since it is a key parameter that can affect the curing variables and, hence, the cross-link density and the final properties of the system. Previous studies of graphene nanofluids [54], formed by a stable suspension of the graphene nanoparticles in a base fluid host, have shown that the thermal conductivity follows a modified effective medium theory developed by Maxwell, which can be reduced to the ratio of the nanofluid thermal conductivity to the thermal conductivity of the base fluid [54]. Figure 8 presents the relative thermal conductivity ($\lambda_{NF}/\lambda_{ER}$, where λ_{NF} is the thermal conductivity of the nanofluid and λ_{ER} is the thermal conductivity of the epoxy resin) and the thermal conductivity enhancement as a function of the loading fraction.

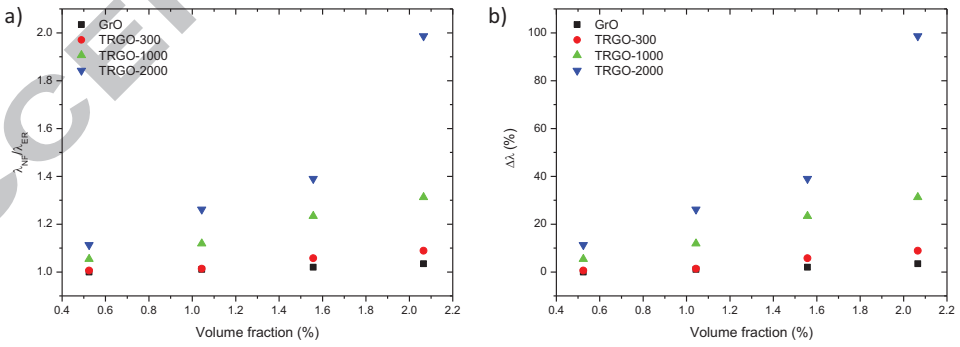

Figure 8. Relative thermal conductivity and thermal conductivity enhancement of the uncured dispersions.

The thermal conductivity of the nanofluids presents a positive trend with both the loading fraction and the annealing temperature. This GrO does not significantly affect the effective thermal conductivity of the system, probably due to the presence of large quantities of oxygen groups in the basal plane. The presence of oxygen groups i.e, epoxy, hydroxyl, carbonyl and carboxylic, can act as scattering point for the phonons through the graphene layers. The reduction of the GrO improves the relative thermal conductivity of the nanofluids (Figure 8.b), up to 9%, 31% and 99% in TRGO-300, TRGO-1000 and TRGO-2000 at 2.06 vol.%, respectively. The improvements of the thermal conductivities for both TRGO-300 and TRGO-1000 are in good agreement with previously reported studies [55]. Meanwhile, the thermal conductivity enhancement observed with TRGO-2000 is among the largest reported in the literature [54]. This dependency of the thermal conductivity with the annealing temperature is related to the resistance to heat flow at the interface, known as Kapitza resistance, which depends on the structural composition and morphology of the graphene materials. Hence, the best performance of the TRGO-2000 sample would be the result of its greater aromatic restoration, the absence of the oxygen groups and the presence of several layers. These characteristics would result in better vibration of the network, minimize coupling losses and improved the transport of phonons between layers [56].

Looking at the cured composite diffusivity, which is proportional to the thermal conductivity, we observed a similar trend with the loading fraction (Figure 9). This almost linear dependency with the loading fraction has previously been reported in various polymer composites [57]. Meanwhile, the dependency with the GM annealing temperature presents a slightly different behavior to that of the uncured state. GrO, TRGO-300 and TRGO-1000 samples have similar diffusivity values, in the 0.12 to 0.17 mm^2/s range. Meanwhile, TRGO-2000 again shows the best performance with

diffusivity enhancements varying from 20 to 142 %. As previously discussed, such different behavior could be related to the absence of the oxygen groups on the surface of the TRGO-2000. While the interaction of the hardener and oxygen groups at the GM/epoxy interfaces could lead to reducing the thermal resistance, the intrinsic thermal conductivity of the filler is decreased with functionalization [57]. The effect of filler functionalization on the thermal conductivity is still a subject of study but, according to the literature, it appears to be more detrimental with scarce studies reporting only marginal enhancement [57].

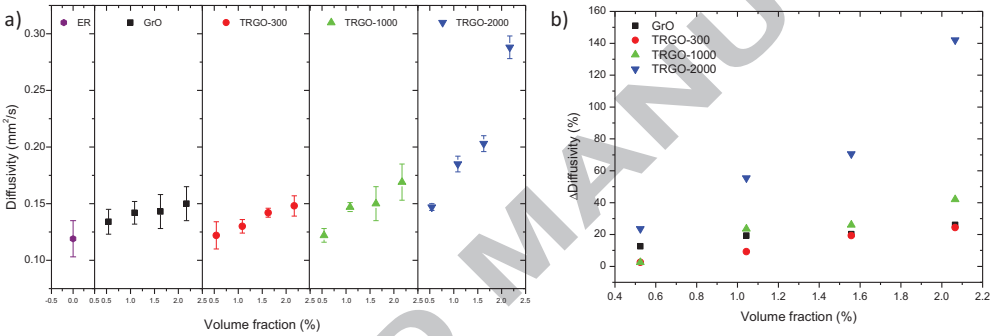

Figure 9. a) Thermal diffusivity and b) thermal diffusivity enhancement of the cured composites

4. Conclusions

The transport properties are strongly influenced by the structural composition and morphology of graphene materials obtained by varying the temperature of the thermal exfoliation/reduction of graphite oxide. The dispersion was analyzed by microscopy techniques in both uncured and cured state. The GMs with high BET surface area show the best dispersion results. Thermal conductivity of composite presents a clear correlation with the structural and chemical composition of GMs, being optimum in case of TRGO-2000 due to high aromatic restoration and structural performance. On the

contrary, the electrical properties are determined by the interaction between the GMs and the dispersion in the polymer. We demonstrated the possibility to modulate the thermal and electric properties by changing the quantity and type of graphene material. The ability to modulate chemical composition and structure of graphene materials and understand the interaction between filled and polymer matrix involved holds significant advantages for the transport application.

Acknowledgments

The authors gratefully acknowledge the financial support of the MINECO, through the project MAT2013-48107-C3. R. Sánchez-Hidalgo thanks to MINECO for the Predoctoral grant BES-2014-070802.

References

[1] F.-L. Jin, X. Li, S.-J. Park, Synthesis and application of epoxy resins: A review, Journal of Industrial and Engineering Chemistry 29 (2015) 1-11.
[2] M. Martin-Gallego, M.M. Bernal, M. Hernandez, R. Verdejo, M.A. Lopez-Manchado, Comparison of filler percolation and mechanical properties in graphene and carbon nanotubes filled epoxy nanocomposites, European Polymer Journal 49 (2013) 1347-1353.
[3] D.V. Pikhurov, V.V. Zuev, The effect of fullerene C60 on the dielectric behaviour of epoxy resin at low nanofiller loading, Chemical Physics Letters 601 (2014) 13-15.
[4] C. Lee, X. Wei, J.W. Kysar, J. Hone, Measurement of the elastic properties and intrinsic strength of monolayer graphene, Science 321 (2008) 385-388.
[5] A.A. Balandin, S. Ghosh, W. Bao, I. Calizo, D. Teweldebrhan, F. Miao, C.N. Lau, Superior thermal conductivity of single-layer graphene, Nano Letters 8 (2008) 902-907.
[6] F. Schedin, A.K. Geim, S.V. Morozov, E.W. Hill, P. Blake, M.I. Katsnelson, K.S. Novoselov, Detection of individual gas molecules adsorbed on graphene, Nature Materials 6 (2007) 652.
[7] C.-C. Teng, C.-C.M. Ma, C.-H. Lu, S.-Y. Yang, S.-H. Lee, M.-C. Hsiao, M.-Y. Yen, K.-C. Chiou, T.-M. Lee, Thermal conductivity and structure of non-covalent functionalized graphene/epoxy composites, Carbon 49 (2011) 5107-5116.
[8] M. Martin-Gallego, R. Verdejo, M.A. Lopez-Manchado, M. Sangermano, Epoxy-graphene UV-cured nanocomposites, Polymer 52 (2011) 4664-4669.

[9] D. Galpaya, M. Wang, G. George, N. Motta, E. Waclawik, C. Yan, Preparation of graphene oxide/epoxy nanocomposites with significantly improved mechanical properties, Journal of Applied Physics 116 (2014) 053518-10.
[10] J. Tang, H. Zhou, Y. Liang, X. Shi, X. Yang, J. Zhang, Properties of graphene oxide/epoxy resin composites, Journal of Nanomaterials 2014 (2014) 1-5.
[11] G.B. Olowojoba, S. Eslava, E.S. Gutierrez, A.J. Kinloch, C. Mattevi, V.G. Rocha, A.C. Taylor, In situ thermally reduced graphene oxide/epoxy composites: thermal and mechanical properties, Applied Nanoscience 6 (2016) 1015-1022.
[12] Z. Anwar, A. Kausar, I. Rafique, B. Muhammad, Advances in epoxy/graphene nanoplatelet composite with enhanced physical properties: A Review, Polymer-Plastics Technology and Engineering 55 (2016) 643-662.
[13] S.G. Prolongo, A. Jiménez-Suárez, R. Moriche, A. Ureña, Graphene nanoplatelets thickness and lateral size influence on the morphology and behavior of epoxy composites, European Polymer Journal 53 (2014) 292-301.
[14] C. Vallés, F. Beckert, L. Burk, R. Mülhaupt, R.J. Young, I.A. Kinloch, Effect of the C/O ratio in graphene oxide materials on the reinforcement of epoxy-based nanocomposites, Journal of Polymer Science Part B: Polymer Physics 54 (2016) 281-291.
[15] R.J. Young, I.A. Kinloch, L. Gong, K.S. Novoselov, The mechanics of graphene nanocomposites: A review, Composites Science and Technology 72 (2012) 1459-1476.
[16] P. Álvarez, C. Blanco, R. Santamaría, P. Blanco, Z. González, L. Fernández-García, U. Sierra, M. Granda, A. Páez, R. Menéndez, Tuning graphene properties by a multi-step thermal reduction process, Carbon 90 (2015) 160-163.
[17] C. Botas, P. Álvarez, P. Blanco, M. Granda, C. Blanco, R. Santamaría, L.J. Romasanta, R. Verdejo, M.A. López-Manchado, R. Menéndez, Graphene materials with different structures prepared from the same graphite by the Hummers and Brodie methods, Carbon 65 (2013) 156-164.
[18] C. Botas, P. Álvarez, C. Blanco, R. Santamaría, M. Granda, P. Ares, F. Rodríguez-Reinoso, R. Menéndez, The effect of the parent graphite on the structure of graphene oxide, Carbon 50 (2012) 275-282.
[19] C. Botas, P. Álvarez, C. Blanco, R. Santamaría, M. Granda, M.D. Gutiérrez, F. Rodríguez-Reinoso, R. Menéndez, Critical temperatures in the synthesis of graphene-like materials by thermal exfoliation-reduction of graphite oxide, Carbon 52 (2013) 476-485.
[20] A.L. Patterson, The Scherrer formula for X-Ray particle size determination, Physical Review 56 (1939) 978-982.
[21] H.-M. Ju, S.H. Huh, S.-H. Choi, H.-L. Lee, Structures of thermally and chemically reduced graphene, Materials Letters 64 (2010) 357-360.
[22] D. Yang, A. Velamakanni, G. Bozoklu, S. Park, M. Stoller, R.D. Piner, S. Stankovich, I. Jung, D.A. Field, C.A. Ventrice Jr, R.S. Ruoff, Chemical analysis of graphene oxide films after heat and chemical treatments by X-ray photoelectron and Micro-Raman spectroscopy, Carbon 47 (2009) 145-152.
[23] A. Ganguly, S. Sharma, P. Papakonstantinou, J. Hamilton, Probing the Thermal Deoxygenation of Graphene Oxide Using High-Resolution In Situ X-ray-based spectroscopies, The Journal of Physical Chemistry C 115 (2011) 17009-17019.
[24] S. Abdolhosseinzadeh, H. Asgharzadeh, H. Seop Kim, Fast and fully-scalable synthesis of reduced graphene oxide, Scientific Reports 5 (2015) 10160.
[25] C. Hontoria-Lucas, A.J. López-Peinado, J.d.D. López-González, M.L. Rojas-Cervantes, R.M. Martín-Aranda, Study of oxygen-containing groups in a series of graphite oxides: Physical and chemical characterization, Carbon 33 (1995) 1585-1592.

[26] J.P. Rourke, P.A. Pandey, J.J. Moore, M. Bates, I.A. Kinloch, R.J. Young, N.R. Wilson, The real graphene oxide revealed: Stripping the oxidative debris from the graphene-like sheets, Angewandte Chemie International Edition 50 (2011) 3173-3177.
[27] M. Acik, C. Mattevi, C. Gong, G. Lee, K. Cho, M. Chhowalla, Y.J. Chabal, The role of intercalated water in multilayered graphene oxide, ACS Nano 4 (2010) 5861-5868.
[28] M. Acik, G. Lee, C. Mattevi, A. Pirkle, R.M. Wallace, M. Chhowalla, K. Cho, Y. Chabal, The role of oxygen during thermal reduction of graphene oxide studied by infrared absorption spectroscopy, The Journal of Physical Chemistry C 115 (2011) 19761-19781.
[29] S.H. Huh, Thermal reduction of graphene oxide, INTECH Open Access Publisher 2011.
[30] S. Stankovich, Synthesis of graphene-based nanosheets via chemical reduction of exfoliated graphite oxide, Carbon 45 (2007) 1558-1565.
[31] A.C. Ferrari, J.C. Meyer, V. Scardaci, C. Casiraghi, M. Lazzeri, F. Mauri, S. Piscanec, D. Jiang, K.S. Novoselov, S. Roth, A.K. Geim, Raman spectrum of graphene and graphene layers, Physical Review Letters 97 (2006) 1-5.
[32] F. Reichert, A.M. Pérez-Mas, D. Barreda, C. Blanco, R. Santamaria, C. Kuttner, A. Fery, N. Langhof, W. Krenkel, Influence of the carbonization temperature on the mechanical properties of thermoplastic polymer derived C/C-SiC composites, Journal of European Ceramic Society 37 (2017) 523-529.
[33] A. Sadezky, H. Muckenhuber, H. Grothe, R. Niessner, U. Pöschl, Raman microspectroscopy of soot and related carbonaceous materials: Spectral analysis and structural information, Carbon 43 (2005) 1731-1742.
[34] S. Vollebregt, R. Ishihara, F.D. Tichelaar, Y. Hou, C.I.M. Beenakker, Influence of the growth temperature on the first and second-order raman band ratios and widths of carbon nanotubes and fibers, Carbon 50 (2012) 3542-3554.
[35] F. Tuinstra, J.L. Koenig, Raman spectrum of graphite, Journal of Chemical Physics 53 (1970) 1126-1130.
[36] R. Konnola, J. Joji, J. Parameswaranpillai, K. Joseph, Structure and thermo-mechanical properties of CTBN-grafted-GO modified epoxy/DDS composites, RSC Advances 5 (2015) 61775-61786.
[37] S. Chatterjee, F. Nafezarefi, N.H. Tai, L. Schlagenhauf, F.A. Nüesch, B.T.T. Chu, Size and synergy effects of nanofiller hybrids including graphene nanoplatelets and carbon nanotubes in mechanical properties of epoxy composites, Carbon 50 (2012) 5380-5386.
[38] M. Martin-Gallego, M. Hernández, V. Lorenzo, R. Verdejo, M.A. Lopez-Manchado, M. Sangermano, Cationic photocured epoxy nanocomposites filled with different carbon fillers, Polymer 53 (2012) 1831-1838.
[39] V.D. Punetha, S. Rana, H.J. Yoo, A. Chaurasia, J.T. McLeskey, M.S. Ramasamy, N.G. Sahoo, J.W. Cho, Functionalization of carbon nanomaterials for advanced polymer nanocomposites: A comparison study between CNT and graphene, Progress in Polymer Science 67 (2017) 1-47.
[40] J. Li, M.L. Sham, J.-K. Kim, G. Marom, Morphology and properties of UV/ozone treated graphite nanoplatelet/epoxy nanocomposites, Composites Science and Technology 67 (2007) 296-305.
[41] D. Toker, D. Azulay, N. Shimoni, I. Balberg, O. Millo, Tunneling and percolation in metal-insulator composite materials, Physical Review B-Condensed Matter and Materials Physics 68 (2003) 041403.

[42] J.M. Vazquez-Moreno, V. Yuste-Sanchez, R. Sanchez-Hidalgo, R. Verdejo, M.A. Lopez-Manchado, L. Fernández-García, C. Blanco, R. Menéndez, Customizing thermally-reduced graphene oxides for electrically conductive or mechanical reinforced epoxy nanocomposites, European Polymer Journal 93 (2017) 1-7.
[43] M.R. Acocella, C.E. Corcione, A. Giuri, M. Maggio, A. Maffezzoli, G. Guerra, Graphene oxide as a catalyst for ring opening reactions in amine crosslinking of epoxy resins, RSC Advances 6 (2016) 23858-23865.
[44] D.R. Dreyer, S. Park, C.W. Bielawski, R.S. Ruoff, The chemistry of graphene oxide, Chemical Society Reviews 39 (2010) 228-240.
[45] H. Chen, V.V. Ginzburg, J. Yang, Y. Yang, W. Liu, Y. Huang, L. Du, B. Chen, Thermal conductivity of polymer-based composites: Fundamentals and applications, Progress in Polymer Science 59 (2016) 41-85.
[46] J.D. Renteria, S. Ramirez, H. Malekpour, B. Alonso, A. Centeno, A. Zurutuza, A.I. Cocemasov, D.L. Nika, A.A. Balandin, Strongly anisotropic thermal conductivity of free-standing reduced graphene oxide films annealed at high temperature, Advanced Functional Materials 25 (2015) 4664-4672.
[47] Y. Huang, Q. Gong, Q. Zhang, Y. Shao, J. Wang, Y. Jiang, M. Zhao, D. Zhuang, J. Liang, Fabrication and molecular dynamics analyses of highly thermal conductive reduced graphene oxide films at ultra-high temperatures, Nanoscale 9 (2017) 2340-2347.
[48] Y. Sun, B. Tang, W. Huang, S. Wang, Z. Wang, X. Wang, Y. Zhu, C. Tao, Preparation of graphene modified epoxy resin with high thermal conductivity by optimizing the morphology of filler, Applied Thermal Engineering 103 (2016) 892-900.
[49] K. Chu, W.-s. Li, H. Dong, Role of graphene waviness on the thermal conductivity of graphene composites, Applied Physics A 111 (2013) 221-225.
[50] X. Shen, Z. Wang, Y. Wu, X. Liu, Y.-B. He, J.-K. Kim, Multilayer graphene enables higher efficiency in improving thermal conductivities of graphene/epoxy composites, Nano Letters 16 (2016) 3585-3593.
[51] T. Zhou, F. Liu, K. Suganuma, S. Nagao, Use of graphene oxide in achieving high overall thermal properties of polymer for printed electronics, RSC Advances 6 (2016) 20621-20628.
[52] Y. Wang, H.F. Zhan, Y. Xiang, C. Yang, C.M. Wang, Y.Y. Zhang, Effect of Covalent functionalization on thermal transport across graphene–polymer interfaces, The Journal of Physical Chemistry C 119 (2015) 12731-12738.
[53] X. Shen, Z. Wang, Y. Wu, X. Liu, J.-K. Kim, Effect of functionalization on thermal conductivities of graphene/epoxy composites, Carbon 108 (2016) 412-422.
[54] E. Sadeghinezhad, M. Mehrali, R. Saidur, M. Mehrali, S. Tahan Latibari, A.R. Akhiani, H.S.C. Metselaar, A comprehensive review on graphene nanofluids: Recent research, development and applications, Energy Conversion and Management 111 (2016) 466-487.
[55] M. Martin-Gallego, R. Verdejo, M. Khayet, J.M.O. de Zarate, M. Essalhi, M.A. Lopez-Manchado, Thermal conductivity of carbon nanotubes and graphene in epoxy nanofluids and nanocomposites, Nanoscale Research Letters 6 (2011) 1-7.
[56] Y.S. Song, J.R. Youn, Influence of dispersion states of carbon nanotubes on physical properties of epoxy nanocomposites, Carbon 43 (2005) 1378-1385.
[57] N. Burger, A. Laachachi, M. Ferriol, M. Lutz, V. Toniazzo, D. Ruch, Review of thermal conductivity in composites: Mechanisms, parameters and theory, Progress in Polymer Science 61 (2016) 1-28.

Supporting Information for

Main structural features of graphene materials controlling the transport properties of epoxy resin-based composites

R. Sánchez-Hidalgo[1,2], V. Yuste-Sanchez[2], R. Verdejo[2], C. Blanco[1],

M.A. Lopez-Manchado[2*], R. Menéndez[1]

[1]*Instituto Nacional del Carbón, INCAR-CSIC, Apartado 73, 33080 Oviedo, Spain*

[2]*Instituto de Ciencia y Tecnología de Polímeros, ICTP-CSIC, C/ Juan de la Cierva 3, 28006-Madrid, Spain*

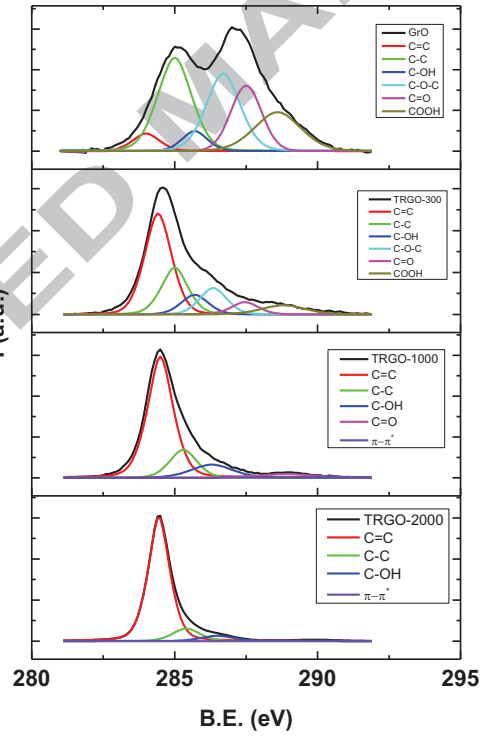

Figure S1. Deconvolution of C1s core-level of the different GMs

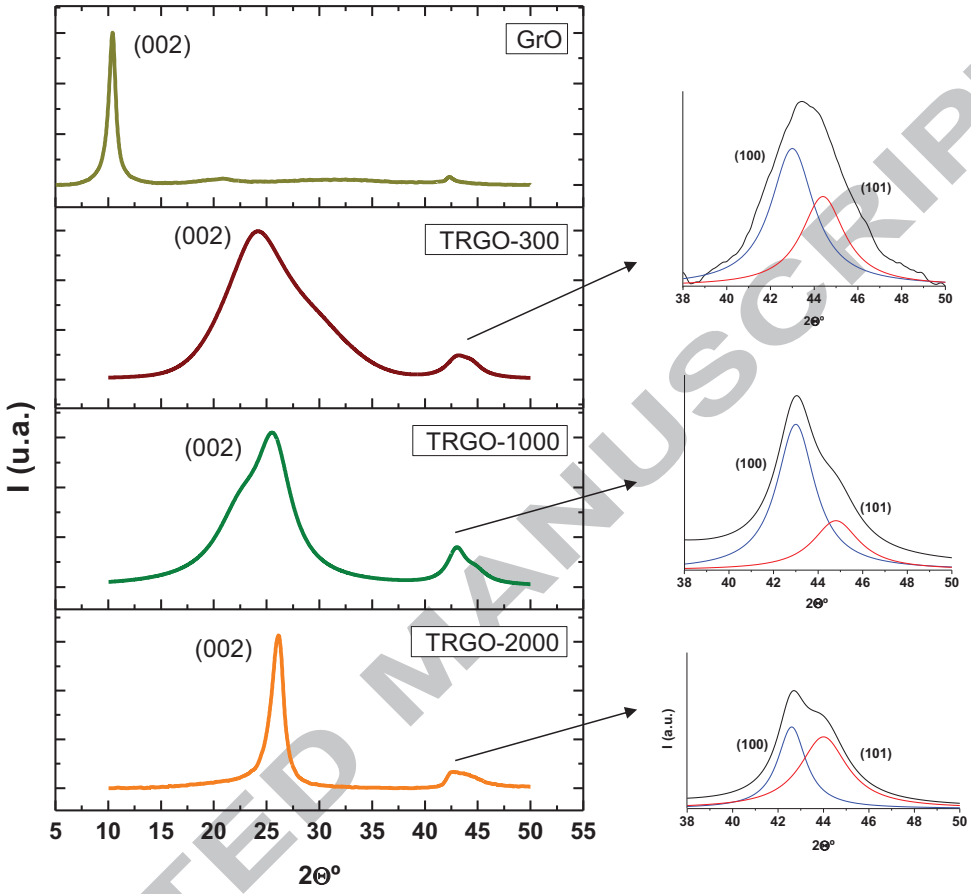

Figure S2. XRD patterns of GMs and the deconvolution of (100) and (101) peaks

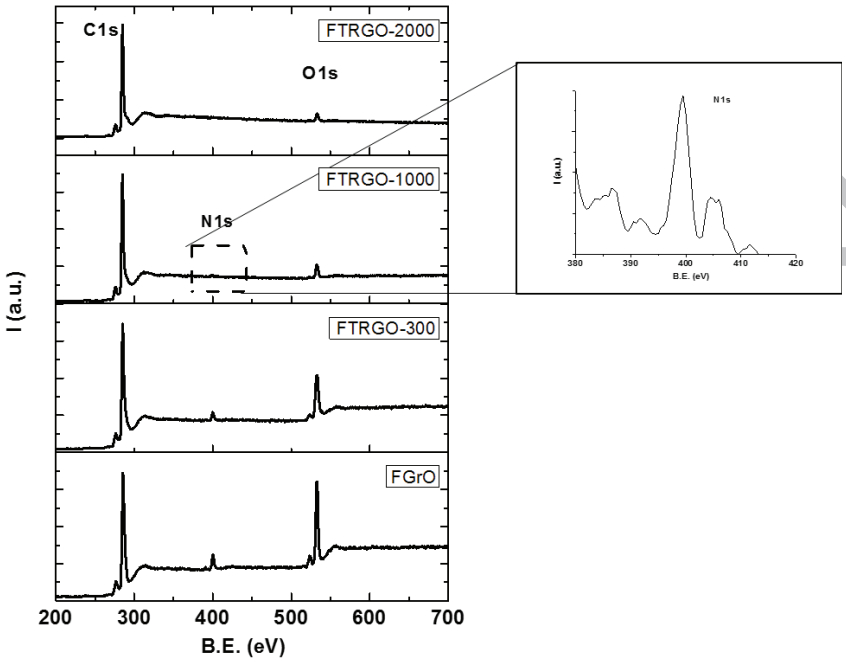

Figure S3. General spectra of XPS measured of GMs

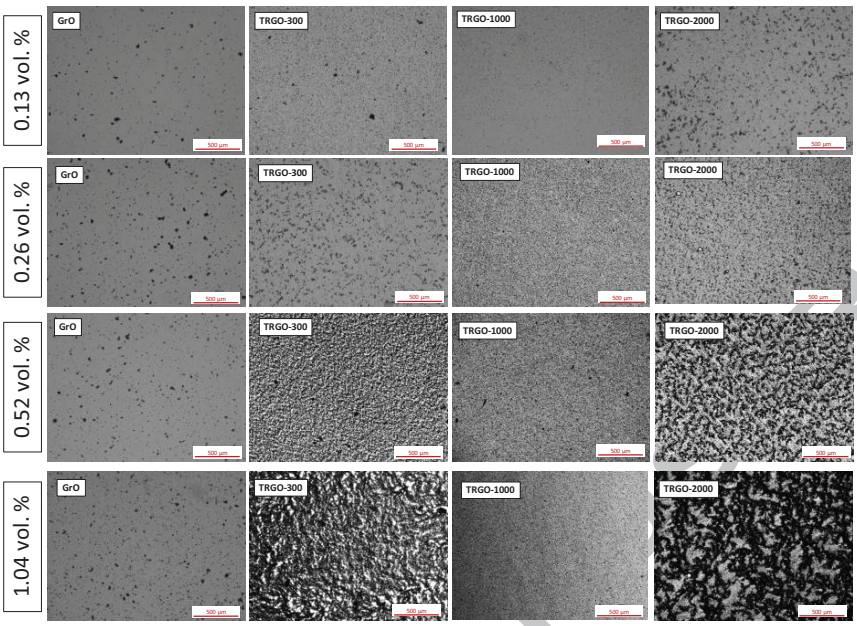

Figure S4. Neat resin dispersion with 0.13 – 1.04 vol. % of GMs

Graphical abstract

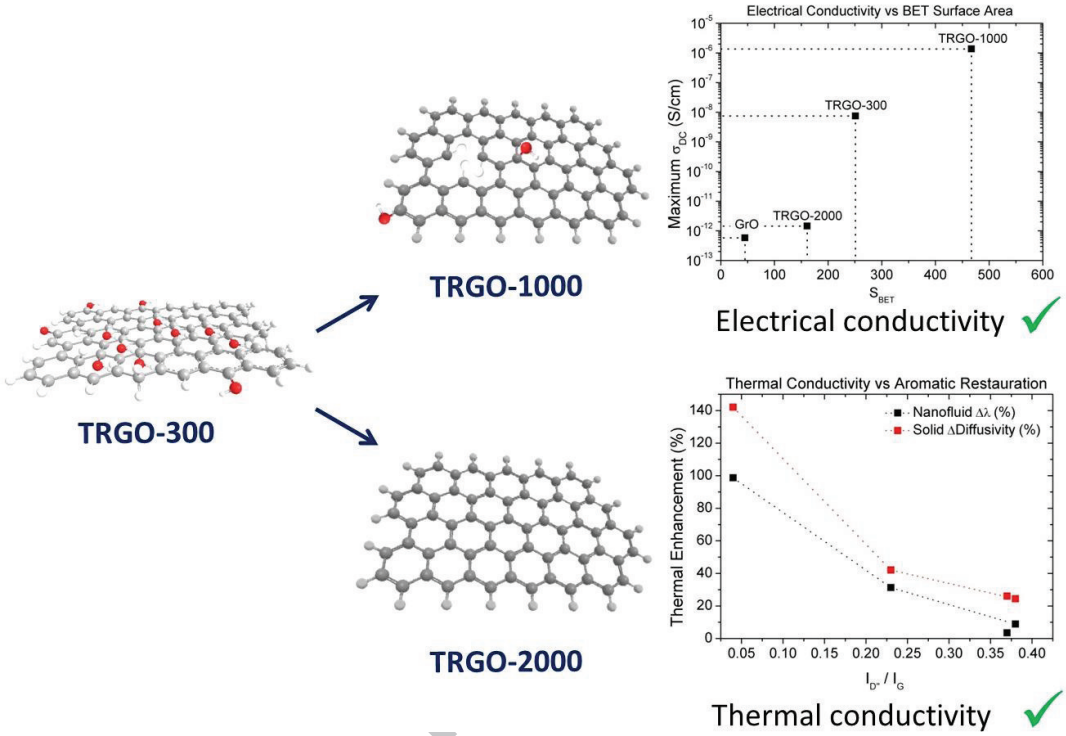

Main structural features of graphene materials controlling the transport properties of epoxy resin-based composites

R. Sánchez-Hidalgo, V. Yuste-Sanchez, R. Verdejo, C. Blanco, M.A. Lopez-Manchado, R. Menéndez

Highlights

- Optimal control of the structure and morphology of graphene materials
- The dispersion of graphene in the epoxy resin is strongly dependent of the BET surface area
- Custom-made graphene-based polymer nanocomposites
- Thermal conductivity benefits from a high aromatic restoration
- Electrical conductivity requires the right balance of filler/matrix interaction and aromatic restoration